JOURNAL OF COMPUTATIONAL PHYSICS 106, 1–18 (1993)

Two Coupled Particle-Finite Volume Methods Using Delaunay–Voronoï Meshes for the Approximation of Vlasov–Poisson and Vlasov–Maxwell Equations

F. HERMELINE

CEA/CEL-V/D. MA/MCN, 94195 Villeneuve Saint Georges Cédex, France

Received August 1, 1990

This paper deals with the approximation of Vlasov–Poisson and Vlasov–Maxwell equations. We present two coupled particle-finite volume methods which use the properties of Delaunay–Voronoï meshes. These methods are applied to benchmark calculations and engineering problems such as simulation of electron injector devices.

1. INTRODUCTION

It is well known that the coupled particle-finite difference method is the most usual tool for the approximation of the Vlasov–Poisson and Vlasov–Maxwell equations (for example, see [1–2]). Unfortunately this method does not really suit arbitrary polygons whose boundaries are not parallel to the axis. Furthermore, it is not easy to vary the mesh size of indented polygons.

In order to overcome these difficulties we present two coupled particle-finite volume methods using unstructured meshes. More precisely we will assume that Ω is covered by a Delaunay mesh [3], which is always possible [4–5]. Algorithms for generating such meshes have been developed in [4–9]. Then some geometrical properties of Delaunay and Voronoï meshes will be used for the approximation of Maxwell equations by two finite volume methods [16]. The Delaunay–Voronoï meshes have been used in such diversified areas as electromagnetics [17–18], semi-conductor physics [19–20], or hydrodynamics [21–22]. For finite difference or finite volume methods solving the Maxwell equations the reader is referred to [23–26]. For other methods such as conformal or mixed finite element and edge element methods see [27–30].

The boundary conditions, stability criteria, application to the wave equation, and generalization to the 3D case will be detailed. Furthermore, we will introduce two finite volume methods for the approximation of the Poisson equation and we will study how the Gauss law can be taken into account when the charge and current densities result from particle calculations.

Some numerical results concerning benchmarks, which permit comparisons between the exact solution and the approximated one, or engineering problems such as injector devices will be presented. Computing various injectors will lead us to propose a direct method for the Child–Langmuir current calculation.

2. MAXWELL EQUATIONS

Given a 2D vector field $\mathbf{V}: R^2 \to R^3$, we set $\mathbf{V} = (V_x, V_y)$ and $V = V_z$. Then the Maxwell equations in S.I. units can be written as

$$\begin{aligned} &\frac{\partial B}{\partial t} + \operatorname{rot} \mathbf{E} = 0 \\ &\frac{\partial \mathbf{E}}{\partial t} - c^2 \,\mathbf{rot}\, B = -\frac{1}{\varepsilon_0}\mathbf{J} \\ &\operatorname{div} \mathbf{E} = \frac{1}{\varepsilon_0}\rho \end{aligned} \tag{1}$$

and

$$\begin{aligned} &\frac{\partial \mathbf{B}}{\partial t} + \mathbf{rot}\, E = 0 \\ &\frac{\partial E}{\partial t} - c^2 \operatorname{rot} \mathbf{B} = -\frac{1}{\varepsilon_0} J \\ &\operatorname{div} \mathbf{B} = 0. \end{aligned} \tag{2}$$

The differential operators are defined in Appendix 1. Let us recall that ρ is the charge density, $\mathbf{J}$ is the current density, c is the velocity of light, and ε_0 is the vacuum permittivity. These values are coupled with the magnetic permeability μ_0 by the relation: $\varepsilon_0 \mu_0 c^2 = 1$.

0021-9991/93 $5.00

We assume that initial electric and magnetic fields $\mathbf{E}^0$ and $\mathbf{B}^0$ are such that:

$$\operatorname{div} \mathbf{E}^0 = \frac{1}{\varepsilon_0}\rho^0 \qquad \text{and} \qquad \operatorname{div} \mathbf{B}^0 = 0.$$

Let $\Gamma = \Gamma_1 \cup \Gamma_2$ be the boundary of Ω. Regarding the boundary conditions we consider:

$$\begin{aligned} \mathbf{E}\cdot\tau &= 0 \\ \mathbf{E}\cdot\tau - cB &= 0 \end{aligned} \qquad \text{(System 1)}$$

and

$$\begin{aligned} E &= 0 \\ E + c\mathbf{B}\cdot\tau &= 0. \end{aligned} \qquad \text{(System 2)}$$

For Γ_1 we recognize the perfect conductor boundary condition. For Γ_2 we have chosen the following simple model:

— the outgoing electromagnetic waves which propagate normally to the boundary Γ can leave freely Ω without being reflected (or equivalently are absorbed at boundary)

— incoming normal waves are allowed to enter Ω.

3. DELAUNAY AND VORONOI MESHES

In this section we recall briefly some properties of the Delaunay and Voronoï meshes. For more details see [3–5, 10–15].

Let $x_1, ..., x_n$ be n points of the plane, not all colinear. With each point x_i we associate the Voronoï polygon (V.P.) V_i defined by

$$V_i = \{x,\ 1 \leqslant j \leqslant n\ d(x, x_i) \leqslant d(x, x_j)\}.$$

It can be proved that $V_1, ..., V_n$ are convex, nonempty interior polygons and that they fit together to fill the whole plane without overlapping. Therefore they make up a mesh of the plane which is called the Voronoï mesh. With each vertex v of one V.P. we associate the convex hull of points among $x_1, ..., x_n$ which have v as one of the vertices of their associated V.P. It can be proved that these so-called Delaunay polygons (D.P.) fit together without overlapping to fill the convex hull of points $x_1, ..., x_n$. Therefore they make up a mesh which is called the Delaunay mesh. Furthermore each D.P. D is inscribed in a closed ball which does not contain any point $x_1, ..., x_n$, except the vertices of D. This last property characterizes the Delaunay mesh.

In the following we will assume that polygon Ω is covered by a submesh of one Delaunay mesh whose vertices have been suitably chosen in Ω. By adding some boundary vertices in case of need it is always possible to obtain such a mesh and algorithms in order to generate it have been developed successfully (see [4–9, 12]). Let us remark that a D.P. or a V.P. may have an arbitrary number of sides. In practice the D.P. will be triangles or rectangles. Typical examples are displayed on the Fig. 1. Other examples can be found in [4, 5, 31].

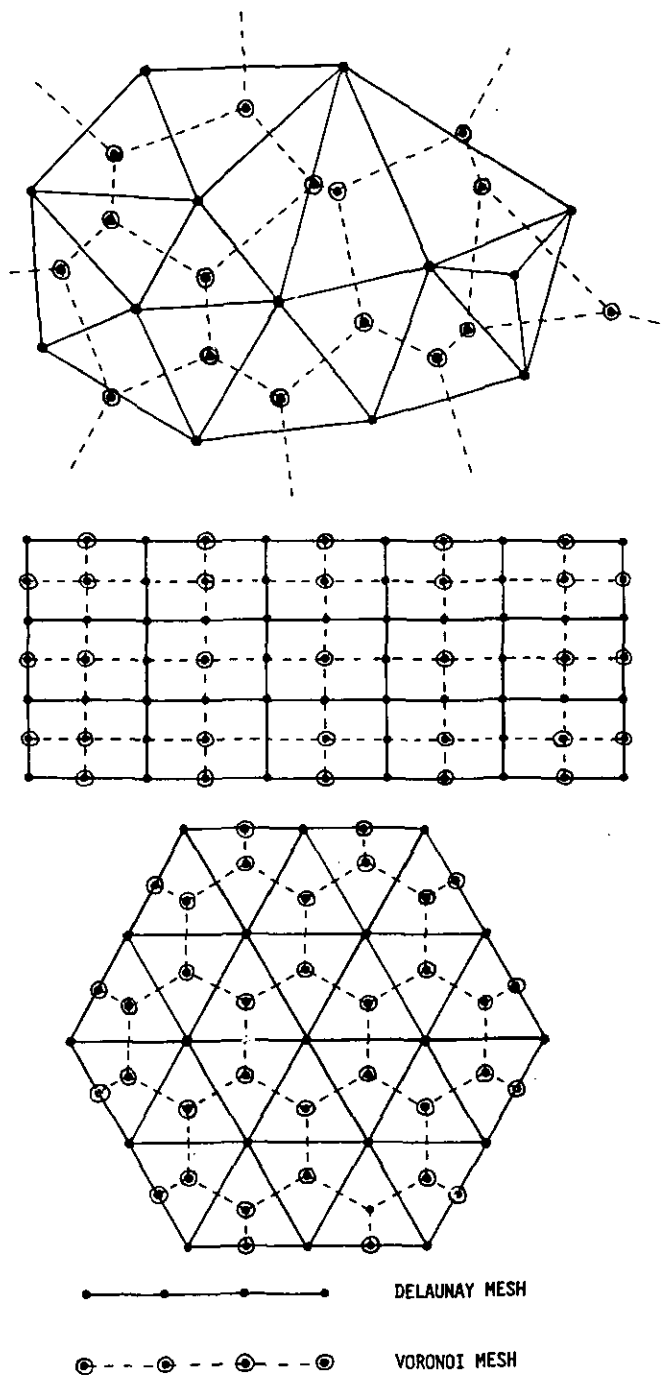

FIGURE 1

A remarkable property of Voronoï and Delaunay meshes is that a unique perpendicular side of one mesh can be associated to each side of the other (see Fig. 1). This is what will make these meshes so attractive for finite volume computations.

In the following index i (j) will be assigned to the V.P. (D.P.). Consequently it will also be assigned to the vertices of D.P. (internal vertices of V.P.). Index k (l) will be assigned to the sides ∂V_i^k (∂D_j^l) of V.P. (D.P.).

Let us denote:

— N_i (N_j) the number of sides of V.P. V_i (D.P. D_j)

— A_i (A_j) the area of V.P. V_i (V.P. D_j)

— L_i^k (L_j^l) and $\bar{L}_i^k$ ($\bar{L}_j^l$) the length of internal side ∂V_i^k (side ∂D_j^l) and its associated side of D.P. (internal side of V.P.)

— $\mathbf{v}_i^k$ ($\mathbf{v}_j^l$) and $\boldsymbol{\tau}_i^k$ ($\boldsymbol{\tau}_j^l$) the unit outward to ∂V_i^k (∂D_j^l) and the unit tangent along ∂V_i^k (∂D_j^l).

If the sides ∂V_i^k and ∂D_j^l are associated we have:

$$L_i^k = \bar{L}_j^l,\ L_j^l = \bar{L}_i^k; \qquad \mathbf{v}_i^k = -\boldsymbol{\tau}_j^l,\ \boldsymbol{\tau}_i^k = \mathbf{v}_j^l.$$

Lastly, let $v(i,k)$ ($v(j,l)$) be the number of the unique V.P. (D.P.) which is adjacent to V_i (D_j) regarding to its k (l) the side. If ∂D_j^l is a boundary side, $v(j,l)$ will denote the number of the V.P.'s vertex which coincides with the middle of side ∂D_j^l (see Fig. 2).

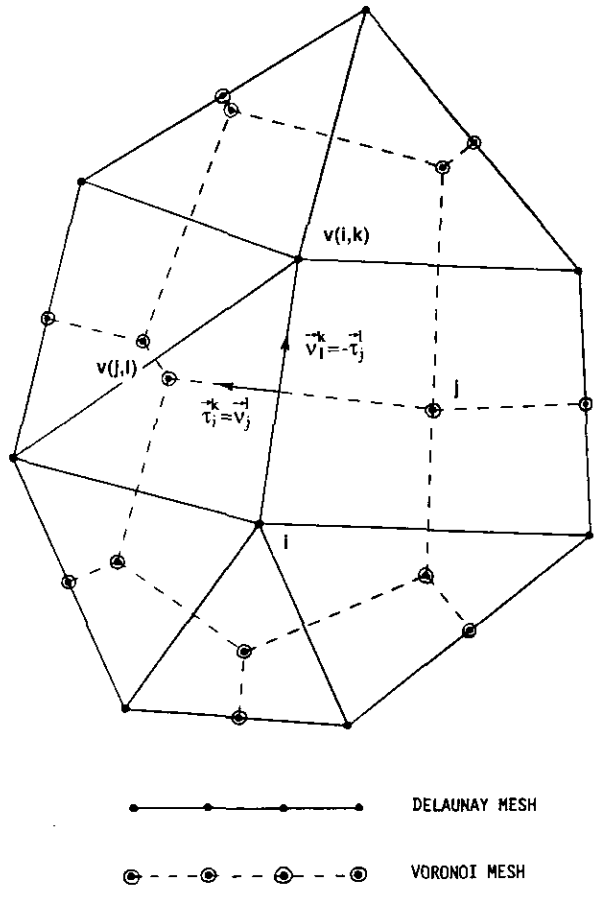

FIGURE 2

4. TWO FINITE VOLUME METHODS FOR THE MAXWELL EQUATIONS

In this section we present and study two finite volume methods for the cartesian 2D Maxwell equations (the cylindrical 2D case is treated in Appendix 2 and the cartesian 3D case is treated in Section 8). These methods generalize the classical finite difference method to arbitrary unstructured Delaunay meshes. The basic idea is to use the fact that the Delaunay and Voronoï meshes are orthogonal. The boundary conditions, stability criteria, and application to the wave equation will be studied.

4.1. *Approximation of the Maxwell Equations*

Consider, for example, Maxwell equations (1) (System (2) is treated in Appendix 3). Integrate the second equation (Ampere law) along side of D.P. ∂D_j^l and integrate the first one (Faraday law) over V.P. V_i and the third one (Gauss law) over D.P. D_j. We obtain

$$\frac{\partial}{\partial t}\left(\int_{V_i} B\right) + \sum_{k=1}^{N_i} \int_{\partial V_i^k} \mathbf{E}\cdot\boldsymbol{\tau}_i^k = 0$$

$$\frac{\partial}{\partial t}\left(\int_{\partial D_j^l} \mathbf{E}\cdot\mathbf{v}_j^l\right) - c^2 \int_{\partial D_j^l} \nabla B\cdot\boldsymbol{\tau}_j^l = -\frac{1}{\varepsilon_0}\int_{\partial D_j^l} \mathbf{J}\cdot\mathbf{v}_j^l$$

$$\sum_{l=1}^{N_j} \int_{\partial D_j^l} \mathbf{E}\cdot\mathbf{v}_j^l = \frac{1}{\varepsilon_0}\int_{D_j} \rho.$$

By exchanging the role played by the Delaunay and Voronoï meshes we obtain

$$\frac{\partial}{\partial t}\left(\int_{D_j} B\right) + \sum_{l=1}^{N_j} \int_{\partial D_j^l} \mathbf{E}\cdot\boldsymbol{\tau}_j^l = 0$$

$$\frac{\partial}{\partial t}\left(\int_{\partial V_i^k} \mathbf{E}\cdot\mathbf{v}_i^k\right) - c^2 \int_{\partial V_i^k} \nabla B\cdot\boldsymbol{\tau}_i^k = -\frac{1}{\varepsilon_0}\int_{\partial V_i^k} \mathbf{J}\cdot\mathbf{v}_i^k$$

$$\sum_{k=1}^{N_i} \int_{\partial V_i^k} \mathbf{E}\cdot\mathbf{v}_i^k = \frac{1}{\varepsilon_0}\int_{V_i} \rho.$$

Suppose that:

— for each V.P. V_i (resp. D.P. D_j) B is a constant $B_i = (1/A_i)\int_{V_i} B$ (resp. $B_j = (1/A_j)\int_{D_j} B$)

— along both associated sides ∂V_i^k and ∂D_j^l, $\mathbf{E}\cdot\mathbf{v}_j^l = \mathbf{E}\cdot\boldsymbol{\tau}_i^k$ (resp. $\mathbf{E}\cdot\mathbf{v}_i^k = -\mathbf{E}\cdot\boldsymbol{\tau}_j^l$) is a constant also denoted by $\mathbf{E}\cdot\mathbf{v}_j^l = \mathbf{E}\cdot\boldsymbol{\tau}_i^k$ (resp. $\mathbf{E}\cdot\mathbf{v}_i^k = -\mathbf{E}\cdot\boldsymbol{\tau}_j^l$).

Thus we have

$$A_i \frac{\partial B_i}{\partial t} + \sum_{k=1}^{N_i} L_i^k \mathbf{E} \cdot \tau_i^k = 0 \tag{3}$$

$$L_j^l \frac{\partial}{\partial t}(\mathbf{E} \cdot \mathbf{v}_j^l) + c^2(B_{v(i,k)} - B_i) = -\frac{1}{\varepsilon_0} \int_{\partial D_j^l} \mathbf{J} \cdot \mathbf{v}_j^l \tag{4}$$

$$\sum_{l=1}^{N_j} L_j^l \mathbf{E} \cdot \mathbf{v}_j^l = \frac{1}{\varepsilon_0} \int_{D_j} \rho \tag{5}$$

(resp.

$$A_j \frac{\partial B_j}{\partial t} + \sum_{l=1}^{N_j} L_j^l \mathbf{E} \cdot \tau_j^l = 0 \tag{6}$$

$$L_i^k \frac{\partial}{\partial t}(\mathbf{E} \cdot \mathbf{v}_i^k) - c^2(B_{v(j,l)} - B_j) = -\frac{1}{\varepsilon_0} \int_{\partial V_i^k} \mathbf{J} \cdot \mathbf{v}_i^k \tag{7}$$

$$\sum_{k=1}^{N_i} L_i^k \mathbf{E} \cdot \mathbf{v}_i^k = \frac{1}{\varepsilon_0} \int_{V_i} \rho \Big). \tag{8}$$

Suppose that the discretized charge conservation law

$$\frac{\partial}{\partial t}\left(\int_{D_j} \rho\right) + \sum_{l=1}^{N_j} \int_{\partial D_j^l} \mathbf{J} \cdot \mathbf{v}_j^l = 0 \tag{9}$$

(resp.

$$\frac{\partial}{\partial t}\left(\int_{V_i} \rho\right) + \sum_{k=1}^{N_i} \int_{\partial V_i^k} \mathbf{J} \cdot \mathbf{v}_i^k = 0\Big) \tag{10}$$

is satisfied. Then, as for the continuous system (1), the discretized Gauss law (5) (resp. (8)) is a consequence of the discretized Ampere law. This is the first advantage of both methods. A second one is that we obtain two linear diagonal systems of differential equations which can be easily integrated by classical methods such as the explicit second-order leapfrog scheme. A third one is that both methods generalize the finite difference method which can be deduced from Eqs. (3)–(5) or (6)–(8) by replacing the D.P. by rectangles (in this case the V.P. are also rectangles, see Fig. 1).

Comparative numerical results are provided in Section 9.1. The second method seems more accurate but we are not yet able to assert that one method must be used rather than the other. However, the stability criterion is more convenient for the first method, due to the fact that the length of D.P.' sides cannot be small (see 4.3).

4.2. *Boundary Conditions*

For the sake of simplicity we will assume that the vertices of V.P. are in the domain Ω. The discretized Faraday law (3) (resp. (6)) requires the calculation of the integral of $\mathbf{E} \cdot \tau_i^k$ (resp. $\mathbf{E} \cdot \tau_j^l$) along $\partial V_i \cap \Gamma$ (resp. $\partial D_j \cap \Gamma$). Now if V_i (resp. D_j) is a boundary V.P. (D.P.) this integral cannot be evaluated from the discretized Ampere law and we have to use the boundary conditions.

Suppose that $\partial V_i \cap \Gamma$ (resp. $\partial D_j \cap \Gamma$) is included in Γ_1. The perfect conductor boundary condition yields

$$\mathbf{E} \cdot \tau_i^k = 0 \qquad \text{on} \quad \partial V_i \cap \Gamma$$

(resp.

$$\mathbf{E} \cdot \tau_j^l = 0 \qquad \text{on} \quad \partial D_j \cap \Gamma).$$

Suppose that $\partial V_i \cap \Gamma$ (resp. $\partial D_j \cap \Gamma$) is included in Γ_2 and let L_i^Γ (resp. L_j^Γ) be the length of $\partial V_i \cap \Gamma$ (resp. $\partial D_j \cap \Gamma$). Since B is a constant B_i (resp. B_j) in V_i (resp. D_j), the integration of the boundary condition

$$\mathbf{E} \cdot \tau - cB = g$$

along $\partial V_i \cap \Gamma$ (resp. $\partial D_j \cap \Gamma$) yields

$$\int_{\partial V_i \cap \Gamma} \mathbf{E} \cdot \tau - cL_i^\Gamma B_i = \int_{\partial V_i \cap \Gamma} g \tag{11}$$

(resp.

$$\int_{\partial D_j \cap \Gamma} \mathbf{E} \cdot \tau - cL_j^\Gamma B_j = \int_{\partial D_j \cap \Gamma} g\Big). \tag{12}$$

The application of the discretized Faraday law (3) (resp. (6)) to V_i (resp. D_j) provides

$$A_i \frac{\partial B_i}{\partial t} + \sum_{\substack{k=1 \\ k \notin \Gamma}}^{N_i} L_i^k \mathbf{E} \cdot \tau_i^k + \int_{\partial V_i \cap \Gamma} \mathbf{E} \cdot \tau = 0 \tag{13}$$

(resp.

$$A_j \frac{\partial B_j}{\partial t} + \sum_{\substack{l=1 \\ 1 \notin \Gamma}}^{N_j} L_j^l \mathbf{E} \cdot \tau_j^l + \int_{\partial D_1 \cap \Gamma} \mathbf{E} \cdot \tau = 0\Big). \tag{14}$$

By replacing (11) (resp. (12)) in (13) (resp. (14)) we obtain the differential equation

$$A_i \frac{\partial B_i}{\partial t} + cL_i^\Gamma B_i + \sum_{\substack{k=1 \\ k \notin \Gamma}}^{N_i} L_i^k \mathbf{E} \cdot \tau_i^k + \int_{\partial V_i \cap \Gamma} g = 0$$

(resp.

$$A_j \frac{\partial B_j}{\partial t} + cL_j^\Gamma B_j + \sum_{\substack{l=1 \\ l \notin \Gamma}}^{N_j} L_j^l \mathbf{E} \cdot \tau_j^l + \int_{\partial D_j \cap \Gamma} g = 0\Big)$$

which allows us to calculate B_i (resp. B_j).

4.3. *Stability Criteria*

Suppose that differential equations (3) and (4) are integrated by the leapfrog scheme and that $\mathbf{J}=0$. We have

$$B_i^{n+1/2}=B_i^{n-1/2}-\frac{\Delta t}{A_i}\sum_{k=1}^{N_i}L_i^k\mathbf{E}^n\cdot\boldsymbol{\tau}_i^k$$

$$\mathbf{E}^{n+1}\cdot\mathbf{v}_j^l=\mathbf{E}^n\cdot\mathbf{v}_j^l+c^2\frac{\Delta t}{L_j^l}(B_i^{n+1/2}-B_{v(i,k)}^{n+1/2}).$$

Let ε_i^k be the error between the approximated electric field component $\mathbf{E}^n\cdot\boldsymbol{\tau}_i^k$ and the exact one. We have

$$B_i^{n+1/2}=B_i^{n-1/2}-\frac{\Delta t}{A_i}\sum_{k=1}^{N_i}L_i^k\mathbf{E}^n\cdot\boldsymbol{\tau}_i^k-\frac{\Delta t}{A_i}\sum_{m=1}^{N_i}L_i^k\varepsilon_i^k;$$

hence

$$\mathbf{E}^{n+1}\cdot\mathbf{v}_j^l=\mathbf{E}^n\cdot\mathbf{v}_j^l+c^2\frac{\Delta t}{L_j^l}(B_i^{n+1/2}-B_{v(i,k)}^{n+1/2})+\eta_j^l$$

with

$$\eta_j^l=c^2\,\Delta t^2\frac{1}{L_j^l}\left(\frac{1}{A_i}\sum_{m=1}^{N_i}L_i^m\varepsilon_i^m-\frac{1}{A_{v(i,k)}}\sum_{m=1}^{N_{v(i,k)}}L_{v(i,k)}^m\varepsilon_{v(i,k)}^m\right).$$

From this relation a sufficient criterion in order that the error does not increase exponentially is

$$c\,\Delta t\left(\frac{1}{L_j^l}\sup\left(\frac{1}{A_i}\sum_{m=1}^{N_i}L_i^m,\frac{1}{A_{v(i,k)}}\sum_{m=1}^{N_{v(i,k)}}L_{v(i,k)}^m\right)\right)^{1/2}<1.$$

Concerning the error between the approximated magnetic field component $B_i^{n+1/2}$ and the exact one, a similar analysis yields

$$c\,\Delta t\left(\frac{1}{A_i}\sum_{k=1}^{N_i}\frac{L_i^k}{\bar{L}_i^k}\right)^{1/2}<1.$$

The numerical experimentation confirms the validity of these criteria. In the case of an orthogonal grid, path Δx, they become

$$c\frac{\Delta t}{\Delta x}<\frac{1}{2}.$$

We observe that this condition is a little more restrictive than the well-known stability criterion

$$c\frac{\Delta t}{\Delta x}<\frac{\sqrt{2}}{2}.$$

Consider now differential equations (6) and (7). A similar analysis leads to the criteria

$$c\,\Delta t\left(\frac{1}{L_i^k}\sup\left(\frac{1}{A_j}\sum_{m=1}^{N_j}L_j^m,\frac{1}{A_{v(j,l)}}\sum_{m=1}^{N_{v(j,l)}}L_{v(j,l)}^m\right)\right)^{1/2}<1 \quad (15)$$

and

$$c\,\Delta t\left(\frac{1}{A_j}\sum_{l=1}^{N_j}\frac{L_j^l}{\bar{L}_j^l}\right)^{1/2}<1. \quad (16)$$

In this case these criteria are too restrictive since the length $L_i^k=\bar{L}_j^l$ of a V.P.'s side may be as small as possible. If there is a V.P.'s side whose length $L_i^k=\bar{L}_j^l$ is such that criteria (15) or (16) are violated, the two D.P.'s D_j and $D_{v(j,l)}$ are replaced by the single polygon $D_j\cup D_{v(j,l)}$. We have

$$B_j^{n+1/2}=B_j^{n-1/2}-\frac{\Delta t}{A_j}\sum_{m=1}^{N_j}L_j^l\mathbf{E}^n\cdot\boldsymbol{\tau}_j^m$$

$$B_{v(j,l)}^{n+1/2}=B_{v(j,l)}^{n-1/2}-\frac{\Delta t}{A_{v(j,l)}}\sum_{m=1}^{N_{v(j,l)}}L_{v(j,l)}^m\mathbf{E}^n\cdot\boldsymbol{\tau}_{v(j,l)}^m.$$

By addition we obtain

$$\begin{aligned}A_jB_j^{n+1/2}+A_{v(j,l)}B_{v(j,l)}^{n+1/2}&=A_jB_j^{n-1/2}+A_{v(j,l)}B_{v(j,l)}^{n+1/2}\\&\quad-\Delta t\left(\sum_{m=1}^{N_j}L_j^m\mathbf{E}^n\cdot\boldsymbol{\tau}_j^l+\sum_{m=1}^{N_{v(j,l)}}L_{v(j,l)}^m\mathbf{E}^n\cdot\boldsymbol{\tau}_{v(j,l)}^m\right).\end{aligned}$$

This relation suggests replacing B_j and $B_{v(j,l)}$ by the new degree of freedom,

$$\beta_{j,l}=\frac{1}{A_j+A_{v(j,l)}}(A_jB_j+A_{v(j,l)}B_{v(j,l)}),$$

which satisfies the relation

$$\begin{aligned}\beta_{j,l}^{n+1/2}=\beta_{j,l}^{n-1/2}-\frac{\Delta t}{A_j+A_{v(j,l)}}&\left(\sum_{m=1}^{N_j}L_j^m\mathbf{E}^n\cdot\boldsymbol{\tau}_j^m\right.\\&\left.+\sum_{m=1}^{N_{v(j,l)}}L_{v(j,l)}^m\mathbf{E}^n\cdot\boldsymbol{\tau}_{v(j,l)}^m\right).\end{aligned}$$

Note that we do not need degree of freedom $\mathbf{E}^n\cdot\boldsymbol{\tau}_j^l$ which can be suppressed. Since the lengths $L_j^l=\bar{L}_i^k$ cannot be small, this precaution is useless for the first finite volume method.

4.4. *Application to the Wave Equation*

By eliminating $\mathbf{E}\cdot\boldsymbol{\tau}_i^k=\mathbf{E}\cdot\mathbf{v}_j^l$ (resp. $\mathbf{E}\cdot\boldsymbol{\tau}_j^l=-\mathbf{E}\cdot\mathbf{v}_i^k$) between Eqs. (3) and (4) (resp. (6) and (7)), we have

$$A_i\frac{\partial^2 B_i}{\partial t^2}+c^2\sum_{k=1}^{N_i}\frac{L_i^k}{\bar{L}_i^k}(B_i-B_{v(i,k)})=\frac{1}{\varepsilon_0}\sum_{k=1}^{N_i}\int_{\partial V_i^k}\mathbf{J}\cdot\boldsymbol{\tau}_i^k$$

(resp.

$$A_j\frac{\partial^2 B_j}{\partial t^2}+c^2\sum_{l=1}^{N_j}\frac{L_j^l}{\bar{L}_j^l}(B_j-B_{v(j,l)})=\frac{1}{\varepsilon_0}\sum_{l=1}^{N_j}\int_{\partial D_j^l}\mathbf{J}\cdot\boldsymbol{\tau}_j^l\Big).$$

We obtain two finite volume approximations of the wave equation:

$$\frac{\partial^2 B}{\partial t^2}-c^2\,\Delta B=\frac{1}{\varepsilon_0}\operatorname{rot}\mathbf{J}$$

which has been integrated over the V.P. (resp. D.P.).

Similarly, by eliminating B_i (resp. B_j) between Eqs. (3) and (4) (resp. (6) and (7)) we have

$$L_j^l\frac{\partial^2}{\partial t^2}(\mathbf{E}\cdot\mathbf{v}_j^l)-c^2\Big(\frac{1}{A_i}\sum_{m=1}^{N_i}L_i^m\mathbf{E}\cdot\boldsymbol{\tau}_i^k-\frac{1}{A_{v(i,k)}}\sum_{m=1}^{N_{v(i,k)}}L_{v(i,k)}^m\mathbf{E}\cdot\boldsymbol{\tau}_{v(i,k)}^m\Big)=-\frac{1}{\varepsilon_0}\int_{\partial D_j^l}\frac{\partial\mathbf{J}}{\partial t}\cdot\mathbf{v}_j^l$$

(resp.

$$L_i^k\frac{\partial^2}{\partial t^2}(\mathbf{E}\cdot\mathbf{v}_i^k)-c^2\Big(\frac{1}{A_j}\sum_{m=1}^{N_j}L_j^m\mathbf{E}\cdot\boldsymbol{\tau}_j^m-\frac{1}{A_{v(j,l)}}\sum_{m=1}^{N_{v(j,l)}}L_{v(j,l)}^m\mathbf{E}\cdot\boldsymbol{\tau}_{v(j,l)}^m\Big)=-\frac{1}{\varepsilon_0}\int_{\partial V_i^k}\frac{\partial\mathbf{J}}{\partial t}\cdot\mathbf{v}_i^k\Big).$$

We obtain two approximations of the equation:

$$\frac{\partial^2\mathbf{E}}{\partial t^2}+c^2\,\mathbf{rot}(\operatorname{rot}\mathbf{E})=-\frac{1}{\varepsilon_0}\frac{\partial\mathbf{J}}{\partial t}$$

which has been integrated along the sides of D.P. (resp. V.P.). Thus the maxwell equations considered as wave equations are also approximated by the finite volume methods described in 4.1.

5. TWO FINITE VOLUME METHODS FOR THE POISSON EQUATION

This section aims to present and study two finite volume methods using Delaunay–Voronoï meshes for the approximation of the following model Poisson equation:

$$-\Delta\varphi=\frac{1}{\varepsilon_0}\rho\qquad\text{in }\Omega$$
$$\varphi=f\qquad\text{on }\Gamma_1$$
$$\mathbf{v}\cdot\nabla\varphi=g\qquad\text{on }\Gamma_2.$$

Integrate over a V.P. V_i such that $i\notin\Gamma_1$ (resp. D.P. D_j). We have

$$\sum_{\substack{k=1\\k\notin\Gamma_2}}^{N_i}\int_{\partial V_i^k}\mathbf{v}_i^k\cdot\nabla\varphi-\sum_{\substack{k=1\\k\in\Gamma_2}}^{N_i}\int_{\partial V_i^k}g=\frac{1}{\varepsilon_0}\int_{V_i}\rho$$

(resp.

$$\sum_{\substack{l=1\\l\notin\Gamma_2}}^{N_j}\int_{\partial D_j^l}\mathbf{v}_j^l\cdot\nabla\varphi-\sum_{\substack{l=1\\l\in\Gamma_2}}^{N_j}\int_{\partial D_j^l}g=\frac{1}{\varepsilon_0}\int_{D_j}\rho\Big).$$

For each V.P. V_i (resp. D.P. D_j) assume that φ is a constant denoted by φ_i (resp. φ_j). From the approximations,

$$\mathbf{v}_i^k\cdot\nabla\varphi=\frac{1}{\bar{L}_i^k}(\varphi_{v(i,k)}-\varphi_i)\tag{17}$$

(resp.

$$\mathbf{v}_j^l\cdot\nabla\varphi=\frac{1}{\bar{L}_j^l}(\varphi_{v(j,l)}-\varphi_j)\Big),$$

we obtain

$$\sum_{\substack{k=1\\k\notin\Gamma_2}}^{N_i}\frac{L_i^k}{\bar{L}_i^k}(\varphi_i-\varphi_{v(i,k)})+\sum_{\substack{k=1\\v(i,k)\in\Gamma_1}}^{N_i}\frac{L_i^k}{\bar{L}_i^k}\varphi_i=\frac{1}{\varepsilon_0}\int_{V_i}\rho+\sum_{\substack{k=1\\v(i,k)\in\Gamma_1}}^{N_i}\frac{L_i^k}{\bar{L}_i^k}f_{v(i,k)}+\sum_{\substack{k=1\\k\in\Gamma_2}}^{N_i}\int_{\partial V_i^k}g\tag{18}$$

(resp.

$$\sum_{\substack{l=1\\l\notin\Gamma}}^{N_j}\frac{L_j^l}{\bar{L}_j^l}(\varphi_j-\varphi_{v(j,l)})+\sum_{\substack{l=1\\l\in\Gamma_1}}^{N_j}\frac{L_j^l}{\bar{L}_j^l}\varphi_j=\frac{1}{\varepsilon_0}\int_{D_j}\rho+\sum_{\substack{l=1\\l\in\Gamma_1}}^{N_j}\frac{L_j^l}{\bar{L}_j^l}f_{v(j,l)}+\sum_{\substack{l=1\\l\in\Gamma_2}}^{N_j}\int_{\partial D_j^l}g\Big).\tag{19}$$

Thus we obtain two linear systems of equations whose associated matrix $[A]=(a_{pq})$ is symmetric, irreducible and such that

— $\forall p\ a_{pp}>0$

— $\forall p\ a_{pp}\geqslant\sum_{p\neq q}|a_{pq}|$

— $\exists p$ such that $a_{pp}>\sum_{q\neq p}|a_{pq}|$.

From these properties it follows that $[A]$ is positive definite (for example, see [32]).

If the elements of mesh are triangles we remark that the matrix of system (18) is the same as the one we should obtain by a piecewise linear finite element approximation. Method (19) is a new method which has been introduced in [16, 22].

In order to solve these linear systems we have used the Cholesky factorization: comparative numerical results are provided in 9.2. An another efficient method is the diagonal preconditioned conjuguate gradient method which has been used when the initial guess is closed to the solution (see 6.3).

6. APPROXIMATION OF THE COUPLED VLASOV–MAXWELL EQUATION

In numerous problems the charge density ρ and the current density $\mathbf{J}$ are computed from the particle approximation of the distribution function f in the phases space. Let m and q denote the mass and charge of particles, we have

$$\rho = q \int f \, d\mathbf{v}, \qquad \mathbf{J} = q \int \mathbf{v} f \, dv.$$

Under the noncollisional assumption the function f is solution of the Vlasov equation:

$$\frac{\partial f}{\partial t} + \mathbf{v} \cdot \nabla f + \frac{q}{m} (\mathbf{E} + \mathbf{v} \times \mathbf{B}) \nabla_{\mathbf{v}} f = 0.$$

This equation is classicaly approximated by the particle method. Let us recall that the particle method yields a weak approximation $\tilde{f}$ of f as a linear combination of Dirac functions (see [33–34]). In the nonrelativistic cartesian case we have

$$\begin{aligned} \tilde{f}(x, y, v_x, v_y, v_z, t) &= \sum_{p=1}^{N} \omega^p \delta(x - x^p(t)) \, \delta(y - y^p(t)) \\ &\quad \times \delta(v - v_x^p(t)) \, \delta(v - v_y^p(t)) \, \delta(v - v_z^p(t)), \end{aligned} \tag{20}$$

where N is the number of particles, ω^p is the weight of particle p, $\mathbf{x}_p(t) = (x^p(t), y^p(t))$ and $\mathbf{v}^p(t) = (v_x^p(t), v_y^p(t), v_z^p(t))$ are the position and velocity of particle p. The functions $\mathbf{x}^p(t)$ and $\mathbf{v}^p(t)$ are solutions to the equations of motion:

$$\frac{d\mathbf{x}^p}{dt} = \mathbf{v}^p$$

$$\frac{d\mathbf{v}^p}{dt} = \frac{q}{m} (\mathbf{E}^p + \mathbf{v}^p \times \mathbf{B}^p).$$

From (20) we obtain the following weak approximations of ρ and $\mathbf{J}$:

$$\tilde{\rho}(x, y, t) = \sum_{p=1}^{N} \omega^p \delta(x - x^p(t)) \, \delta(y - y^p(t)) \tag{21}$$

$$\tilde{\mathbf{J}}(x, y, t) = \sum_{p=1}^{N} \omega^p \, \mathbf{v}^p(t) \, \delta(x - x^p(t)) \, \delta(y - y^p(t)). \tag{22}$$

Three difficulties arise when we couple the particle method with the finite volume methods described in Section 4.1:

(1) the computation of the electromagnetic field $(\mathbf{E}^p, \mathbf{B}^p)$ acting on particle p

(2) the computation of the flux of the current density $\mathbf{J}$ through the sides of V.P. (or D.P.)

(3) the fact that the discretized charge conservation law (9) or (10) is not necessarily exactly satisfied.

These three items will be dealt with in the next three paragraphs. For the sake of simplicity we will assume that all D.P. are triangles.

6.1. *Fields Interpolation*

The electromagnetic field is interpolated by piecewise linear functions. In order to approximate the magnetic field component B at the ith vertex of the mesh from the degrees of freedom of the first (resp. second) finite volume method we set

$$B(i) = B_i = \frac{1}{A_i} \int_{V_i} B$$

(resp.

$$B(i) = \frac{\sum_{j \in J_i} A_j B_j}{\sum_{j \in J_i} A_j} \Big),$$

where J_i is the set of D.P. whose i is a vertex.

In order to approximate the electric field $\mathbf{E}$ from the degrees of freedom $E \cdot \tau_i^k = \mathbf{E} \cdot \mathbf{v}_j^l$ (resp. $\mathbf{E} \cdot \mathbf{v}_i^k = -\mathbf{E} \cdot \tau_j^l$) we use the least squares method. Therefore $\mathbf{E}(i)$ is the value which minimizes the function:

$$F_i(\mathbf{V}) = \sum_{k=1}^{N_i} (\mathbf{V} \cdot \tau_i^k - \mathbf{E} \cdot \tau_i^k)^2$$

(resp.

$$F_i(\mathbf{V}) = \sum_{k=1}^{N_i} (\mathbf{V} \cdot \mathbf{v}_i^k - \mathbf{E} \cdot \mathbf{v}_i^k)^2 \Big).$$

6.2. *Computation of Current Density Fluxes*

The current density $\mathbf{J}$ is also interpolated by piecewise linear functions. Let φ_i be the piecewise linear function such that

$$\forall_j, \qquad \varphi_i(j) = \delta_{ij}.$$

We set

$$\mathbf{J}(i) = \frac{\int_\Omega \mathbf{J}\,\varphi_i}{\int_\Omega \varphi_i}.$$

From the particle approximation (22) we deduce:

$$\mathbf{J}(i) = \frac{\sum_{p=1}^{N} \mathbf{v}^p\,\varphi_i(\mathbf{x}^p)}{\int_\Omega \varphi_i}. \tag{23}$$

From this piecewise linear interpolation of $\mathbf{J}$ we can easily calculate the fluxes:

$$\int_{\partial D_j^l} \mathbf{J}\cdot\mathbf{v}_j^l \qquad \text{or} \qquad \int_{\partial V_i^k} \mathbf{J}\cdot\mathbf{v}_i^k.$$

Another way of computing these values consists in setting

$$\mathbf{J}\cdot\mathbf{v}_j^l = \frac{1}{\Delta t\, L_j^l}\int_{t-\Delta t/2}^{t+\Delta t/2}\int_{\partial D_j^l}\mathbf{J}\cdot\mathbf{v}_j^l = \frac{1}{\Delta t\, L_j^l}\sum_{p\in P_j^l}\omega^p \tag{24}$$

or

$$\mathbf{J}\cdot\mathbf{v}_i^k = \frac{1}{\Delta t\, L_i^k}\int_{t-\Delta t/2}^{t+\Delta t/2}\int_{\partial V_i^k}\mathbf{J}\cdot\mathbf{v}_i^k = \frac{1}{\Delta t\, L_i^k}\sum_{p\in P_i^k}\omega^p, \tag{25}$$

where P_j^l (P_i^k) is the set of particles which have crossed the side ∂D_j^l (∂V_i^k) between times $t-\Delta t/2$ and $t+\Delta t/2$.

6.3. *Poisson Correction*

Let us assume that the charge density ρ is the piecewise linear function which interpolates the values:

$$\rho(i) = \sum_{p=1}^{N}\varphi_i(\mathbf{x}^p)\Big/\int_\Omega \varphi_i. \tag{26}$$

Unfortunately the discretized charge conservation law (9) or (10) is not exactly satisfied when the piecewise linear approximations (23) and (26) are used. We deduce that the discretized Gauss law is not a consequence of the discretized Ampere law anymore. In order to avoid accumulating errors it is necessary to correct the electric field at any time by adding the gradient of potential φ such that

$$\operatorname{div}(\mathbf{E}-\nabla\varphi) = \frac{1}{\varepsilon_0}\rho.$$

Therefore we have to solve:

$$-\Delta\varphi = \frac{1}{\varepsilon_0}\rho - \operatorname{div}\mathbf{E} \qquad \text{in } \Omega$$

$$\varphi = 0 \qquad \text{on } \Gamma.$$

From the previous finite volume approximation (18) (resp. (19)) and since $\mathbf{E}\cdot\mathbf{v}_i^k$ (resp. $\mathbf{E}\cdot\mathbf{v}_j^l$) is a constant along ∂V_i^k (resp. ∂D_j^l) we obtain

$$\sum_{\substack{k=1\\ k\notin\Gamma}}^{N_i}\frac{L_i^k}{\bar L_i^k}(\varphi_i-\varphi_{v(i,k)}) + \sum_{\substack{k=1\\ v(i,k)\in\Gamma}}^{N_i}\frac{L_i^k}{\bar L_i^k}\varphi_i = \frac{1}{\varepsilon_0}\int_{V_i}\rho - \sum_{k=1}^{N_i} L_i^k\mathbf{E}\cdot\mathbf{v}_i^k$$

(resp.

$$\sum_{\substack{l=1\\ l\notin\Gamma}}^{N_j}\frac{L_j^l}{\bar L_j^l}(\varphi_j-\varphi_{v(j,l)}) + \sum_{\substack{l=1\\ v(j,l)\in\Gamma}}^{N_j}\frac{L_j^l}{\bar L_j^l}\varphi_j = \frac{1}{\varepsilon_0}\int_{D_j}\rho - \sum_{l=1}^{N_j} L_j^l\mathbf{E}\cdot\mathbf{v}_j^l\Big).$$

In order to solve these linear systems it is convenient to use iterative methods such as the diagonal preconditionned conjuguate gradient method because the initial guess (potential at the previous time) is closed to the solution. The numerical experimentation confirms that few iterations are needed (see [30]). Similar results have been presented in [35].

Once these linear systems are solved the former values $\mathbf{E}\cdot\mathbf{v}_i^k$ (resp. $\mathbf{E}\cdot\mathbf{v}_j^l$) of the electric field are replaced by the new corrected values:

$$\mathbf{E}\cdot\mathbf{v}_i^k + \frac{1}{\bar L_i^k}(\varphi_i-\varphi_{v(i,k)})$$

(resp.

$$\mathbf{E}\cdot\mathbf{v}_j^l + \frac{1}{\bar L_j^l}(\varphi_j-\varphi_{v(j,l)})\Big).$$

On the other hand, the discretised charge conservation law (9) or (10) is clearly satisfied if the approximation (24) or (25) of the current density fluxes are used. In this case the discretized Gauss law remains a consequence of the discretized Ampere law and we do not need to correct the electric field. This would be a decisive advantage but it is known that approximations (24) or (25) provide noisy results, especially in the case of plasma computations, and they have not been yet implemented.

7. THE CHILD–LANGMUIR CURRENT CALCULATION

Simulation models of various physical systems such as particle injectors require accurate computation of the Child–Langmuir current density of electrons emitted through the cathode. The aim of this section is to present an algorithm for computing this current density without using the Child–Langmuir law. Of course we shall use the coupled particle-finite volume methods which has been described.

Let us consider the following Vlasov–Poisson model equation:

$$\frac{\partial f}{\partial t}+\mathbf{v}\cdot\nabla f+\frac{e}{m}\nabla\varphi\cdot\nabla_{\mathbf{v}} f=0$$

$$f(\mathbf{x},\mathbf{v},0)=0 \qquad \text{in } \Omega$$

$$-\Delta\varphi=-\frac{e}{\varepsilon_0}\int f\,d\mathbf{v} \qquad \text{in } \Omega$$

$$\varphi=0 \qquad \text{on the cathode } \Gamma_1$$

$$\varphi=\varphi_A \qquad \text{on the anode.}$$

We make the basic assumption that the net current density at the cathode is space charge limited and hence calculated from the supplementary boundary condition:

$$\mathbf{v}\cdot\nabla\varphi=0 \qquad \text{on the cathode } \Gamma_1.$$

This assumption is equivalent to the one used in the Child–Langmuir model (see [36]) with the advantage of being local and applicable to any geometry. For example, integrate the Poisson equation over a D.P. V_i which intersects Γ_1 and assume that

$$\mathbf{v}_i^k\cdot\nabla\varphi=\frac{1}{\bar{L}_i^k}(\varphi_{v(i,k)}-\varphi_i).$$

Since $\varphi_i=0$ and $\mathbf{v}_i^k\cdot\nabla\varphi=0$ along Γ_1, we have

$$\sum_{\substack{k=1\\ k\notin\Gamma}}^{N_i}\frac{L_i^k}{\bar{L}_i^k}\varphi_{v(i,k)}=\frac{1}{\varepsilon_0}\int_{V_i}\rho. \tag{27}$$

In order to take into account the supplementary cathode boundary condition $\mathbf{v}\cdot\nabla\varphi=0$, relation (27) suggests the following algorithm:

— Given N^n particles, weight ω^n, positions $\mathbf{x}^n$ at time $n\,\Delta t$, the charge density ρ^n is computed.

— From ρ^n the Poisson equation yields φ^n.

— From (27), a prediction $Q_{i,p}^n$ of the charge which must exist in V_i for the supplementary cathode boundary condition to be ensured is then

$$Q_{i,p}^n=-\varepsilon_0\sum_{\substack{k=1\\ k\notin\Gamma}}^{N_i}\frac{L_i^k}{\bar{L}_i^k}\varphi_{v(i,k)}.$$

— The actual charge $Q_{i,a}^n$ in V_i is computed:

$$Q_{i,a}^n=\int_{V_i}\rho^n.$$

— Both charges $Q_{i,a}^n$ and $Q_{i,p}^n$ are compared with intent to compute the charge Q_i^n which must be added through $\partial V_i\cap\Gamma_1$ at time $n\,\Delta t$:

$$Q_i^n=0 \qquad \text{if } |Q_{i,p}^n|\leqslant|Q_{i,a}^n|$$

$$Q_i^n=Q_{i,p}^n-Q_{i,a}^n \qquad \text{otherwise.}$$

— The additional charge Q_i^n is distributed among N^{n+1} new particles which are randomly set on $\partial V_i\cap\Gamma_1$. Their velocities are computed from the cathode temperature.

— The old particles are moved according to the equation of motion in the self-consistent electric field and the new particles are moved according to their initial velocities.

— The new charge density ρ^{n+1} is computed.

This algorithm can be generalized easily to full Maxwell equations. For theoretical results regarding the convergence of such a similar algorithm to the Child–Langmuir current density we refer to [37].

8. GENERALIZATION TO THE 3D CASE

Let Ω be an arbitrary 3D polyhedron. Suppose that Ω is covered by Delaunay and Voronoï meshes and let us denote:

— ∂V_i^k (∂D_j^l) the kth (lth) face of V.P. V_i (D.P. D_j)

— $\partial V_i^{k,r}$ ($\partial D_j^{l,s}$) the rth (sth) edge of the kth (lth) face of V.P. V_i (D.P. D_j)

— N_i (N_j) the number of faces of V.P. V_i (D.P. D_j)

— N_i^k (N_j^l) the number of edges of face ∂V_i^k (∂D_j^l)

— A_i^k (A_j^l) the area of face ∂V_i^k (∂D_j^l)

— $L_i^{k,r}$ ($L_j^{l,s}$) the length of edge $\partial V_i^{k,r}$ ($\partial V_j^{l,s}$)

— $\mathbf{v}_i^k$ ($\mathbf{v}_j^l$) the unit outward normal to ∂V_i^k (∂D_j^l) and $\tau_i^{k,r}$ ($\tau_j^{l,s}$) the unit tangent along edge $\partial V_i^{k,r}$ ($\partial D_j^{l,s}$).

We remark that a unique perpendicular edge of D.P.

(V.P.) can be associated to each face of V.P. (D.P.) (see Fig. 3). Consider the 3D Maxwell equations in S.I. units:

$$\frac{\partial \mathbf{B}}{\partial t} + \mathbf{rot}\,\mathbf{E} = 0$$

$$\frac{\partial \mathbf{E}}{\partial t} - c^2\,\mathbf{rot}\,\mathbf{B} = -\frac{1}{\varepsilon_0}\mathbf{J}$$

$$\operatorname{div}\mathbf{E} = \frac{1}{\varepsilon_0}\rho$$

$$\operatorname{div}\mathbf{B} = 0.$$

Integrate the first (resp. second) equation over a face of V.P. ∂V_i^k (resp. D.P. ∂D_j^l) and integrate the third (resp. fourth) one over a D.P. D_j (resp. V.P. V_i). From Stokes and Gauss theorems we obtain

$$\frac{\partial}{\partial t}\left(\int_{\partial V_i^k} \mathbf{B}\cdot\mathbf{v}_i^k\right) + \sum_{r=1}^{N_i^k} \int_{\partial V_i^{k,r}} \mathbf{E}\cdot\boldsymbol{\tau}_i^{k,r} = 0$$

$$\frac{\partial}{\partial t}\left(\int_{\partial D_j^l} \mathbf{E}\cdot\mathbf{v}_j^l\right) - c^2 \sum_{s=1}^{N_j^l} \int_{\partial D_j^{l,s}} \mathbf{B}\cdot\boldsymbol{\tau}_j^{l,s} = -\frac{1}{\varepsilon_0}\int_{\partial D_j^l} \mathbf{J}\cdot\mathbf{v}_j^l$$

$$\sum_{l=1}^{N_j} \int_{\partial D_j^l} \mathbf{E}\cdot\mathbf{v}_j^l = \frac{1}{\varepsilon_0}\int_{D_j} \rho$$

$$\sum_{k=1}^{N_i} \int_{\partial V_i^k} \mathbf{B}\cdot\mathbf{v}_i^k = 0.$$

Assume that

— along both face ∂V_i^k and its associated perpendicular edge $\partial D_j^{l,s}$, $\mathbf{B}\cdot\mathbf{v}_i^k = \mathbf{B}\cdot\boldsymbol{\tau}_j^{l,s}$ is a constant also denoted by $\mathbf{B}\cdot\mathbf{v}_i^k = \mathbf{B}\cdot\boldsymbol{\tau}_j^{l,s}$

— along both face ∂D_j^l and its associated perpendicular edge $\partial V_i^{k,r}$, $\mathbf{E}\cdot\mathbf{v}_j^l = \mathbf{E}\cdot\boldsymbol{\tau}_i^{k,r}$ is a constant also denoted by $\mathbf{E}\cdot\mathbf{v}_j^l = \mathbf{E}\cdot\boldsymbol{\tau}_i^{k,r}$.

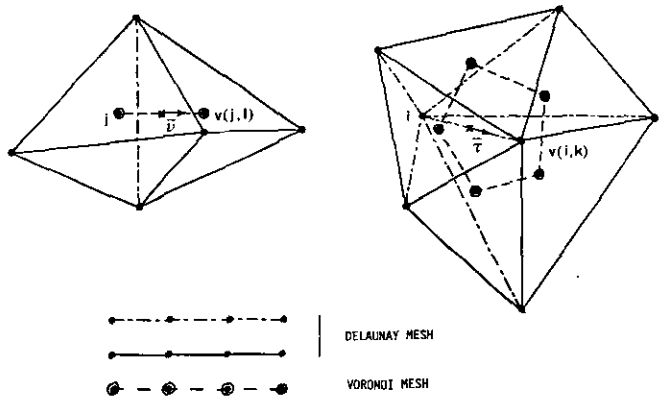

FIGURE 3

Then we have

$$A_i^k \frac{\partial}{\partial t}(\mathbf{B}\cdot\mathbf{v}_i^k) + \sum_{r=1}^{N_i^k} L_i^{k,r}\mathbf{E}\cdot\boldsymbol{\tau}_i^{k,r} = 0 \tag{28}$$

$$A_j^l \frac{\partial}{\partial t}(\mathbf{E}\cdot\mathbf{v}_j^l) - c^2 \sum_{s=1}^{N_j^l} L_j^{l,s}\mathbf{B}\cdot\boldsymbol{\tau}_j^{l,s} = -\frac{1}{\varepsilon_0}\int_{\partial D_j^l} \mathbf{J}\cdot\mathbf{v}_j^l \tag{29}$$

$$\sum_{l=1}^{N_j} A_j^l \mathbf{E}\cdot\mathbf{v}_j^l = \frac{1}{\varepsilon_0}\int_{D_j} \rho \tag{30}$$

$$\sum_{k=1}^{N_i} A_i^k \mathbf{B}\cdot\mathbf{v}_i^k = 0. \tag{31}$$

If the discretized charge conservation law

$$\frac{\partial}{\partial t}\left(\int_{D_j} \rho\right) + \sum_{l=1}^{N_j} \int_{\partial D_j^l} \mathbf{J}\cdot\mathbf{v}_j^l = 0$$

is satisfied, Eq. (30) is a consequence of (29) and is not to be considered. Similarly Eq. (31) is a consequence of (28). Thus we obtain a linear diagonal system of differential equations which can be integrated by classical methods such as the leapfrog scheme.

By exchanging the role played by the Delaunay and Voronoï meshes we obtain a second finite volume approximation of the Maxwell equations. As we have seen in the 2D case these methods generalize the finite difference method (also called Yee's method, see [23]) to arbitrary Delaunay meshes.

The unique drawback of such methods is that they need a Delaunay mesh of polyhedron Ω. Such meshes have been already generated but this remains a challenge to conceive an algorithm which works for any arbitrary polyhedron (see [4, 5, 7, 8]). In order to overcome this difficulty it is possible to use modified finite volume techniques which can be applied to nonorthogonal staggered meshes (see [26]).

9. NUMERICAL RESULTS

In this section we present numerical results involving the Poisson and Maxwell equations or the coupled Vlasov–Poisson and Vlasov–Maxwell equations.

9.1. *Eigenmodes of a Square Cavity*

Let Ω be the unit square. Positive integers m, n and frequency ω are given such that

$$\omega = \pi c(m^2 + n^2)^{1/2}.$$

The electromagnetic field,

$$B(x, y, t) = \cos(\pi mx)\cos(\pi ny)\cos(\omega t)$$

$$\mathbf{E}(x, y, t) = \frac{c}{(m^2+n^2)^{1/2}}(-n\cos(\pi mx)\sin(\pi ny),$$
$$m\sin(\pi mx)\cos(\pi ny))\sin(\omega t),$$

is the solution to the Maxwell equations,

$$\frac{\partial B}{\partial t} + \text{rot } \mathbf{E} = 0$$
$$\frac{\partial \mathbf{E}}{\partial t} - c^2 \,\mathbf{rot}\, B = 0 \qquad \text{in} \quad \Omega \times [0, T]$$

$$B(x, y, 0) = \cos(\pi mx)\cos(\pi ny)$$
$$\mathbf{E}(x, y, 0) = 0 \qquad \text{in } \Omega.$$
$$\mathbf{E} \cdot \tau = 0 \qquad \text{on } \Gamma.$$

We have chosen $m = n = 1$ (hence $\omega = 1.33 \times 10^9\ \text{s}^{-1}$), $T = 40$ ns, and $\Delta t = 20$ ps. Two kinds of mesh have been tested (see Fig. 4):

— a regular orthogonal grid which is made up of 2500 squares such that $\Delta x = \Delta y = 2$ cm

— an unstructured Delaunay mesh which is made up of 5520 triangles and which coïncide with the former along the boundary (due to the mesh generation algorithm the symmetry is not necessary to obtain good results).

Figure 4 shows the error between the analytic solution and

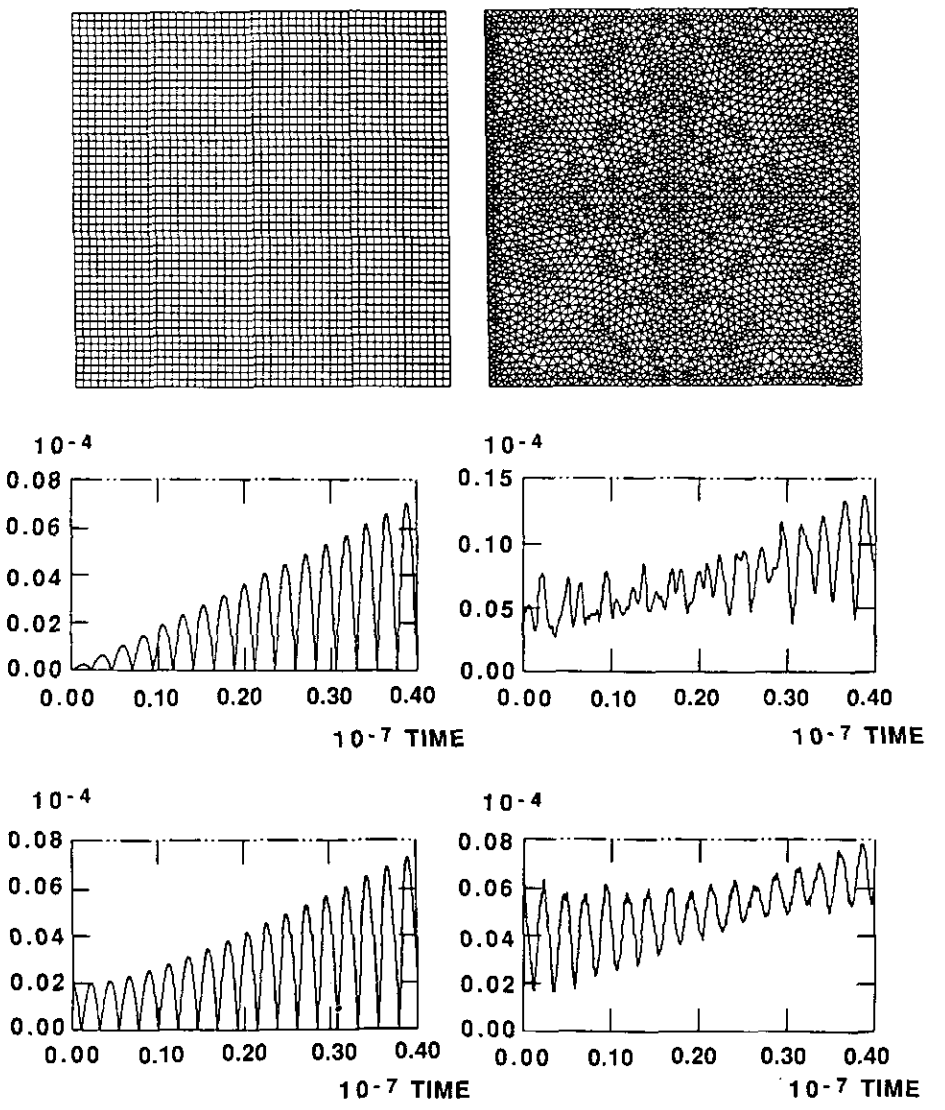

FIGURE 4

the approximated one for both finite volume methods described in Section 4. We have checked the error in the discrete L^2 norm. Note that the error scale varies from plot to plot.

9.2. *A Model Poisson Equation*

Let Ω be the unit square. Positive integers m, n being given the function

$$\varphi(x, y) = \cos(\pi mx) + \sin(\pi ny)$$

is the solution to the model Poisson equation:

$$-\Delta\varphi = \pi^2(m^2 \cos(\pi mx) + n^2 \sin(\pi ny))$$
$$\varphi(x, 0) = \varphi(x, 1) = \cos(\pi mx)$$
$$\mathbf{v} \cdot \nabla\varphi(0, y) = \mathbf{v} \cdot \nabla\varphi(1, y) = 0.$$

We have chosen $m = n = 1$ and the two meshes of Fig. 4 have been tested. The following table displays the error in the discrete L^2 norm between the analytic solution and the

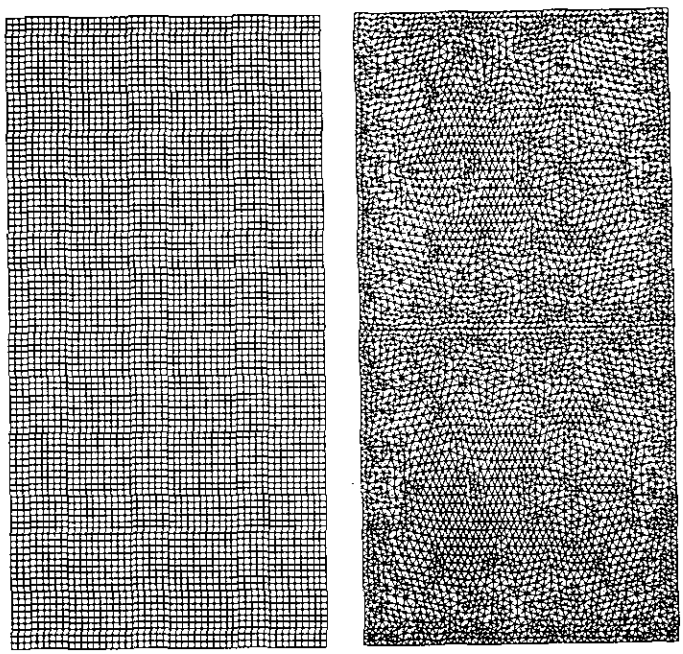

FIGURE 5

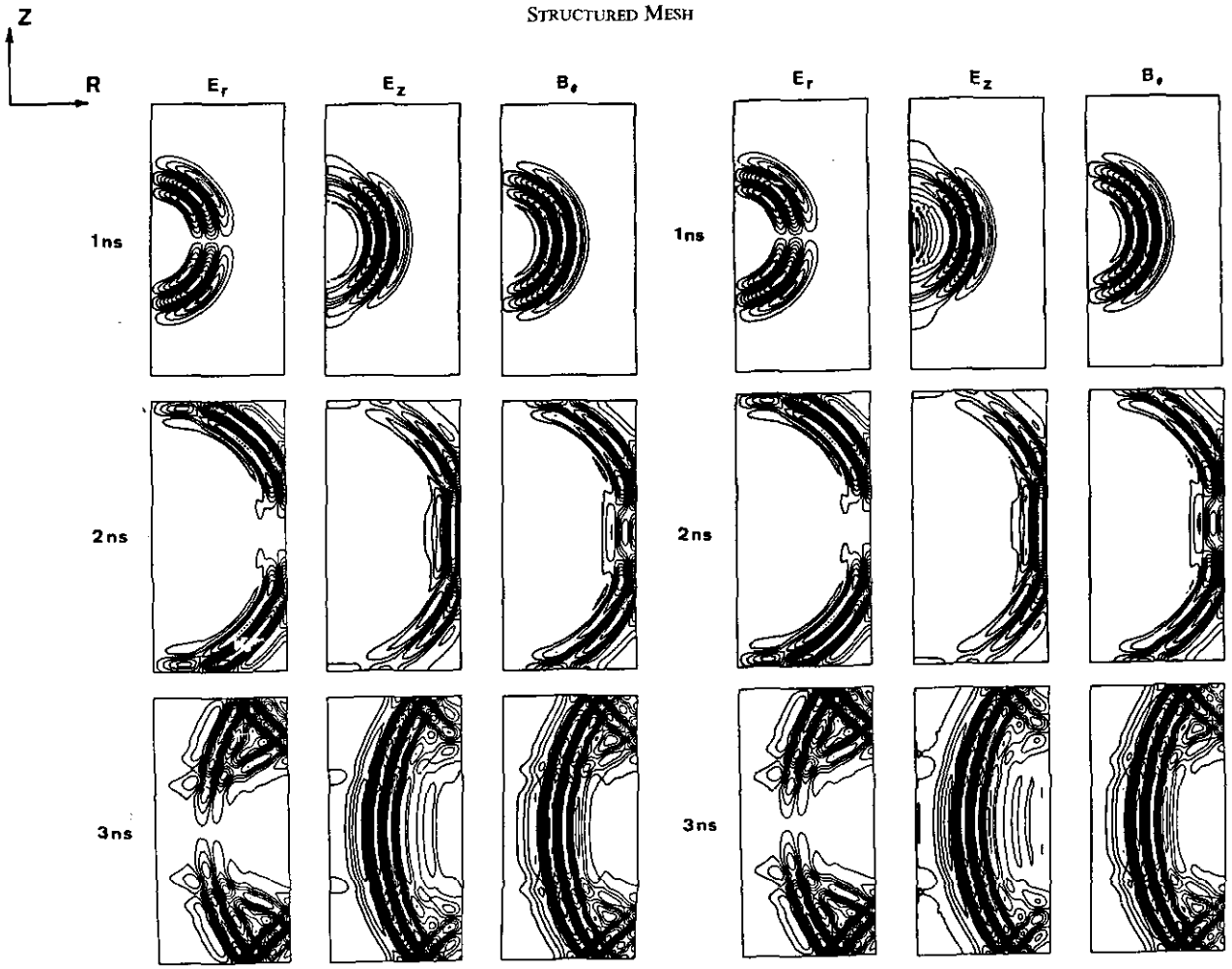

FIGURE 6

approximated one for both finite volume methods described in Section 5.

	Method (18)	Method (19)
Structured mesh	4.96×10^{-6}	5.10×10^{-6}
Unstructured mesh	3.33×10^{-6}	5.05×10^{-6}

9.3. *Radiation from a Dipole*

Let $\Omega = [0, 0.5] \times [-0.5, 0.5]$ and consider the cylindrical Maxwell equations:

$$\frac{\partial B}{\partial t} + \operatorname{rot} \mathbf{E} = 0$$

$$\frac{\partial \mathbf{E}}{\partial t} - c^2 \operatorname{\mathbf{rot}} B = -\frac{1}{\varepsilon_0}\mathbf{J} \qquad \text{in} \quad \Omega \times [0, T]$$

$$B(r, z, 0) = 0$$

$$\mathbf{E}(r, z, 0) = 0 \qquad \text{in } \Omega$$

$$B = 0$$

$$\mathbf{E} \cdot \mathbf{v} = 0 \qquad \text{on the } z\text{-axis}$$

$$\mathbf{E} \cdot \tau = 0 \qquad \text{on } \Gamma,$$

where

$$\mathbf{J}(r, z, t) = \left(0, \left(1 - \frac{(r^2 + z^2)^{1/2}}{R}\right) \sin(\omega t)\right)$$

$$\text{if} \quad 0 \leqslant t \leqslant \frac{2\pi}{\omega} \text{ and } (r^2 + z^2)^{1/2} \leqslant R$$

$$\mathbf{J}(r, z, t) = 0 \qquad \text{otherwise.}$$

We have chosen $T = 3$ ns, $\Delta t = 5$ ps, $\omega = 5\pi\, 10^9\ \mathrm{s}^{-1}$, $R = 4$ cm. Two kinds of mesh have been tested (see Fig. 5):

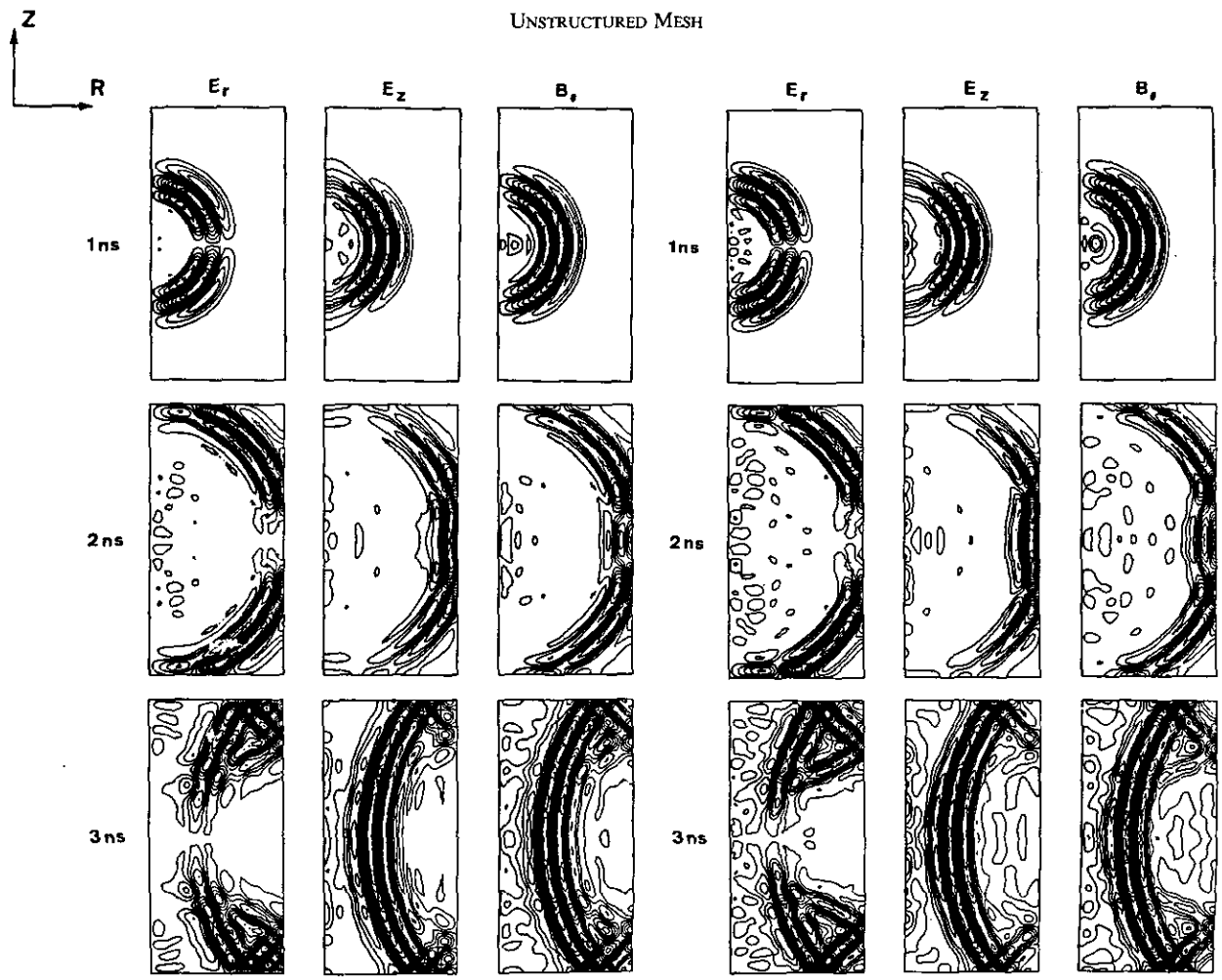

FIGURE 7

— a regular orthogonal grid which is made up of 5000 squares such that $\Delta r = \Delta z = 1$ cm

— an unstructured Delaunay mesh which is made up of 9480 triangles and which coïncide with the former along the boundary (due to the mesh generation algorithm the up–down symmetry is not necessary to obtain good results).

Figures 6 and 7 display the computed contour plot of the electromagnetic field components E_r, E_z, B_θ for times 1 ns, 2 ns, 3 ns with both finite volume methods described in Section 4.

Similar results have been obtained in the cartesian case (see [38]).

9.4. *Numerical Simulation of a Thermal Cathode*

Let us consider the Pierce gun [39] defined by Fig. 8. Let

$$\mathbf{p} = \left(1 - \frac{v^2}{c^2}\right)^{-1/2} \mathbf{v}$$

be the velocity momentum. This Pierce gun is governed by the cylindrical relativistic Vlasov–Poisson equations:

$$\frac{\partial f}{\partial t} + \mathbf{v} \cdot \nabla f + \frac{e}{m}(\nabla \varphi - \mathbf{v} \times \mathbf{B}) \cdot \nabla_{\mathbf{p}} f = 0 \quad \text{in} \quad \Omega \times [0, T]$$

$$f(r, z, v_r, v_z, 0) = 0 \quad \text{in } \Omega$$

$$-\Delta \varphi = -\frac{e}{\varepsilon_0} \int f \, d\mathbf{v} \quad \text{in } \Omega$$

$$\varphi = 0 \quad \text{on the cathode}$$

$$\varphi = \varphi_E \quad \text{on the focusing electrode}$$

$$\varphi = \varphi_A \quad \text{on the anode}$$

$$\mathbf{v} \cdot \nabla \varphi = 0 \quad \text{on the } z\text{-axis}$$

$$\mathbf{rot}\, B = -e\mu_0 \int \mathbf{v} f \, dv \quad \text{in } \Omega.$$

We have chosen $\varphi_E = 1.5 \times 10^6$ V, $\varphi_A = 3 \times 10^6$ V, $T = 4$ ns, $\Delta t = 10$ ps, and the cathode temperature is 2000°K. We have used the Delaunay mesh of Fig. 8 which is made up of 9174 triangles whose size is $\Delta z = 2$ mm on the z-axis. We have entered 100 particles per time step.

The computed Child–Langmuir current is 911 A. Figure 9 shows the electrons in the pipe and the computed contour lines of the potential and azimuthal magnetic field. For such static case computations using coupled particle finite difference or finite element methods see [40–41].

9.5. *Numerical Simulation of a Photo-Injector*

Consider the model photo-injector defined by (see Fig. 10):

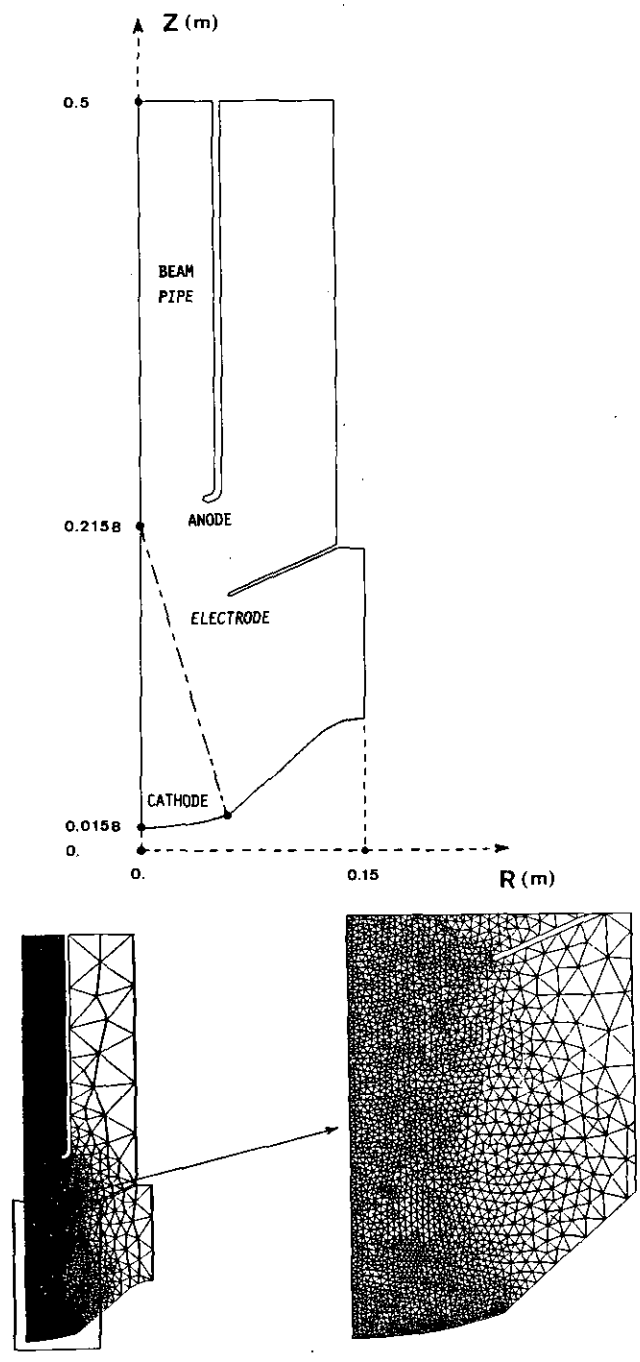

FIGURE 8

— a plane cathode (C), area 1 cm^2, emitting a bunch of photo-current

— a R.F. cavity (RF) which gives an electric field E_z^{RF} such that

$$E_z^{RF}(r, z, t) = E_0(1 + az^2) \cos^2\left(\frac{\pi}{2}\frac{z}{z_0}\right) \cos(\omega t + \varphi)$$

$$\text{if} \quad 0 \leqslant z \leqslant z_0$$

$$E_z^{RF}(r, z, t) = 0 \quad \text{otherwise}$$

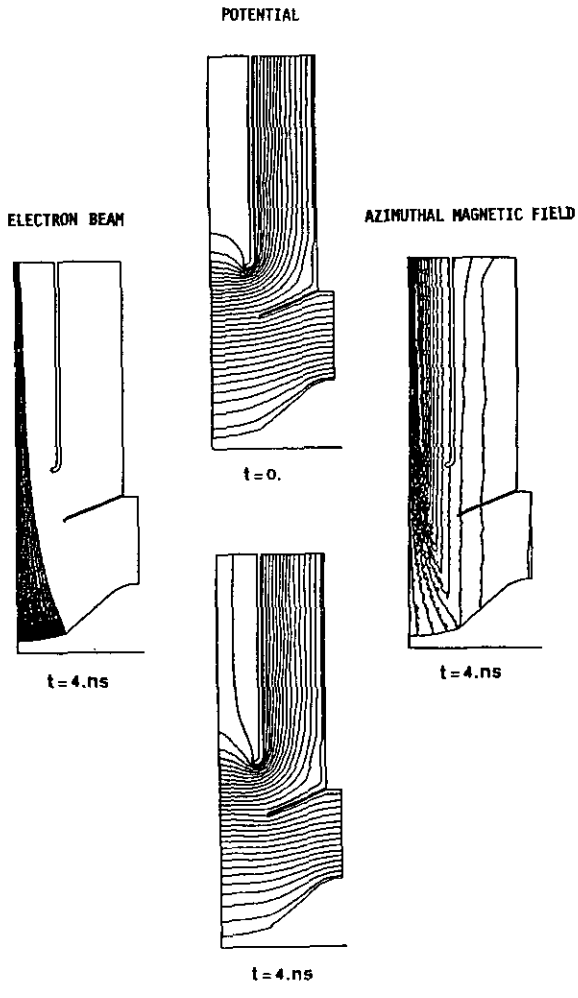

FIGURE 9

(such an analytic expression is a crude fit of the TM01 mode calculated by a standard eigenmode code used for the R.F. cavity)

— a beam pipe (BP)

— a magnetic lens (ML) which gives a magnetic field B_z^{ML} such that

$$B_z^{\mathrm{ML}}(r, z) = \frac{B_0}{2}\left(1 + \cos\left(\pi \frac{2z - z_2 - z_1}{z_2 - z_1}\right)\right) \quad \text{if} \quad z_1 \leqslant z \leqslant z_2$$
$$B_z^{\mathrm{ML}}(r, z) = 0 \quad \text{otherwise.}$$

(this expression intends to approximate crudely the field given by a real coil with magnetic core; a more sophisticated approximation could obviously be used as needed).

We have chosen $E_0 = 1.5 \times 10^7$ V/m, $B_0 = 0.08$, 0.1, 0.12 T, $a = 270\ \mathrm{m}^{-2}$, $z_0 = 10$ cm, $z_1 = 3$ cm, $z_2 = 22$ cm, $\omega = 9.073\ 10^8\ \mathrm{s}^{-1}$, and $\varphi = 0$. From the equations

$$\operatorname{div} \mathbf{E}^{\mathrm{RF}} = 0 \qquad \text{and} \qquad \operatorname{div} \mathbf{B}^{\mathrm{ML}} = 0,$$

we deduce the analytical expression of E_r^{RF} and B_r^{ML}.

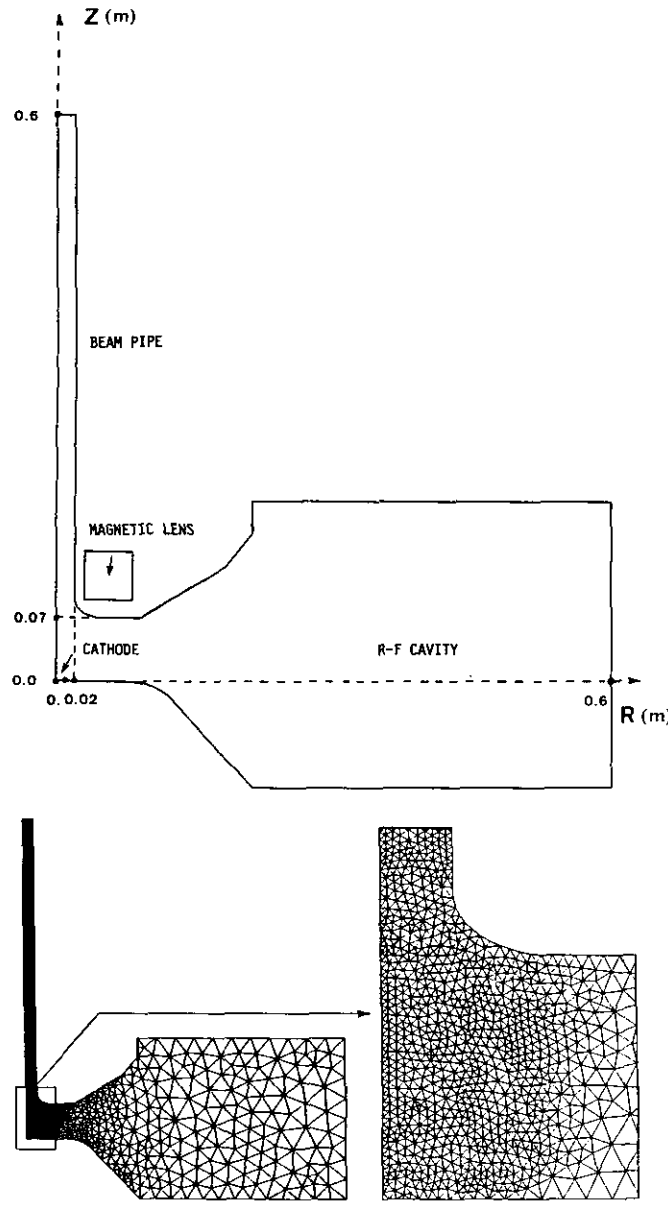

FIGURE 10

Furthermore, we will assume that $B_0^{\mathrm{RF}} = 0$, where the beam is present (r small). Let

$$\mathbf{p} = \left(1 - \frac{v^2}{c^2}\right)^{-1/2} \mathbf{v}$$

denote the velocity momentum. This photo-injector is governed by the cylindrical relativistic Vlasov–Maxwell equations:

$$\frac{\partial f}{\partial t} + \mathbf{v} \cdot \nabla f - \frac{e}{m}(\mathbf{E} + \mathbf{E}^{\mathrm{RF}} + \mathbf{v} \times (\mathbf{B} + \mathbf{B}^{\mathrm{ML}}))$$
$$\cdot \nabla_{\mathbf{p}} f = 0 \qquad \text{in} \quad \Omega \times [0, T]$$

$$f(r, z, v_r, v_\theta, v_z, 0) = 0 \qquad \text{in } \Omega$$

$$\frac{\partial B}{\partial t} + \text{rot } \mathbf{E} = 0$$

$$\frac{\partial \mathbf{B}}{\partial t} + \mathbf{rot}\ E = 0$$

$$\frac{\partial \mathbf{E}}{\partial t} + c^2\ \mathbf{rot}\ B = -\frac{1}{\varepsilon_0}\int \mathbf{v} f\, \mathrm{d}\mathbf{v} \qquad \text{in} \quad \Omega \times [0, T]$$

$$\frac{\partial E}{\partial t} + c^2\ \text{rot}\ \mathbf{B} = -\frac{1}{\varepsilon_0}\int v f\, dv$$

$$B(r, z, 0) = 0$$

$$\mathbf{B}(r, z, 0) = 0 \qquad \text{in } \Omega$$

$$\mathbf{E}(r, z, 0) = 0$$

$$E(r, z, 0) = 0$$

$$B = \mathbf{B} \cdot \mathbf{v} = 0$$

$$E = \mathbf{E} \cdot \mathbf{v} = 0 \qquad \text{on the } z\text{-axis.}$$

We have chosen $T = 2$ ns and $\Delta t = 10$ ps. We have used the Delaunay mesh of Fig. 10 which is made up of 7541

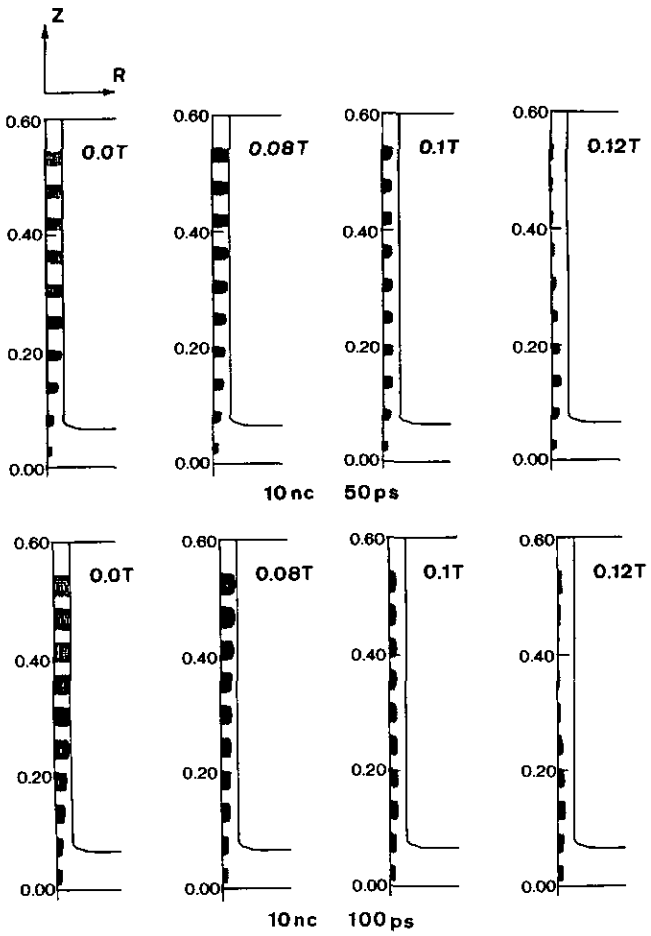

FIG. 11. Space time evolution of the electron bunch under various conditions.

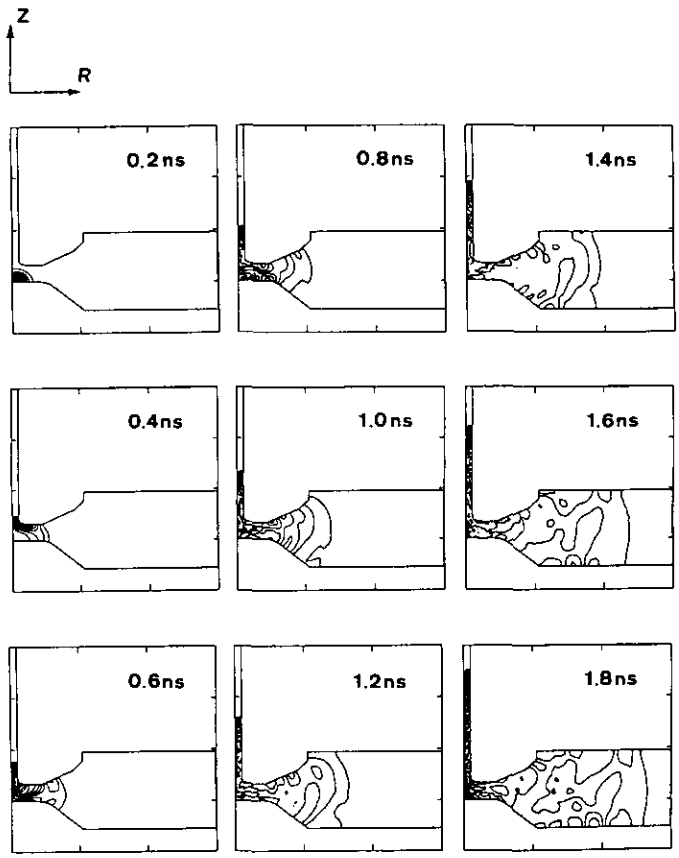

FIG. 12. Contour lines of the azimuthal magnetic field.

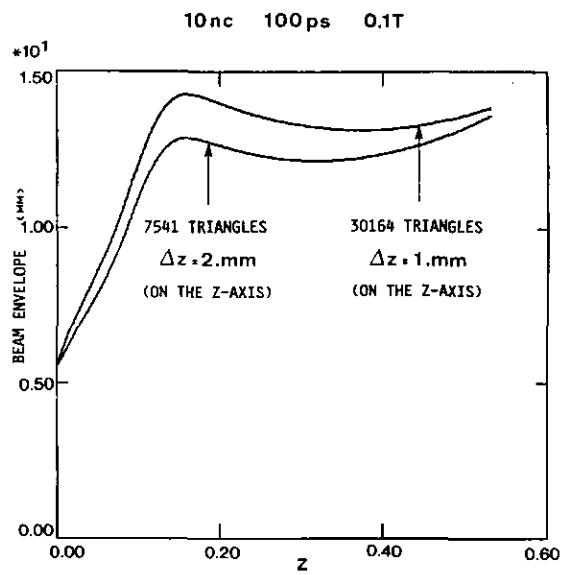

FIG. 13. Influence of the mesh size on the beam envelope.

triangles whose size is $\Delta z = 2$ mm on the z-axis. We have entered 15 particles per time step. The total bunch charge is 10^{-8} Cb with durations 50 ps and 100 ps.

Figure 11 shows the electrons in the pipe for time 0.2 ns to 2 ns by step 0.2 ns under various physical conditions. Figure 12 shows the computed contour lines of the azimuthal wakefield. Figure 13 shows the influence of the mesh size on the beam envelope (the finest mesh is obtained by dividing each triangle in 4). For such computations using coupled particle-finite element methods see [30, 42].

10. IMPLEMENTATION

Both finite volume methods described in paragraph 4 have been easily vectorized. The vectorization of the particle method on unstructured meshes is a little more difficult (see [30]).

Comparison was done with a fully vectorized particle-finite difference code. On a CRAY-XMP type computer the cost of the particle pusher of both codes is about 10 μs per particle and per time step (including assignment and interpolation). The cost of the finite volume code is about 15 μs per grid point and per time step (including the Poisson correction which has not been yet vectorized). This cost is several times higher than for the finite difference code in terms of μs per grid point but, due to the unstructured mesh versatility, the number of grid points is much lower, so the total cost is about the same.

11. CONCLUSION

We have shown that both coupled particle-finite volume methods described in this paper are very suited to approximate the Vlasov–Poisson and Vlasov–Maxwell equations on arbitrary complicated polygons. Numerous advantages have been brought to light. On the other hand, the unique requirement is the need for using Delaunay and Voronoï meshes, which is not a constraint anymore in the 2D case. The application of these methods to various engineering problem has given quite satisfactory results for a cost which can be compared with that of the classical particle-finite difference method. Furthermore both finite volume methods have been generalized to arbitrary physical mediums without any difficulty.

APPENDIX 1

We recall the definitions of some cartesian and cylindrical 2D differential operators.

Cartesian geometry	Cylindrical geometry
$u = u(x, y)$	$u = u(r, z)$
$\mathbf{V}u = \left(\frac{\partial u}{\partial x}, \frac{\partial u}{\partial y}\right)$	$\mathbf{V}u = \left(\frac{\partial u}{\partial r}, \frac{\partial u}{\partial z}\right)$
$\mathbf{rot}\, u = \left(\frac{\partial u}{\partial y}, -\frac{\partial u}{\partial x}\right)$	$\mathbf{rot}\, u = \left(-\frac{\partial u}{\partial z}, \frac{1}{r}\frac{\partial}{\partial r}(ru)\right)$
$\Delta u = \frac{\partial^2 u}{\partial x^2} + \frac{\partial^2 u}{\partial y^2}$	$\Delta u = \frac{1}{r}\frac{\partial}{\partial r}\left(r\frac{\partial u}{\partial r}\right) + \frac{\partial^2 u}{\partial z^2}$
$\mathbf{V} = (V_x(x, y), V_y(x, y))$	$\mathbf{V} = (V_r(r, z), V_z(r, z))$
$\operatorname{div} \mathbf{V} = \frac{\partial V_x}{\partial x} + \frac{\partial V_y}{\partial y}$	$\operatorname{div} \mathbf{V} = \frac{1}{r}\frac{\partial}{\partial r}(rV_r) + \frac{\partial V_z}{\partial z}$
$\mathbf{rot}\, \mathbf{V} = -\frac{\partial V_x}{\partial y} + \frac{\partial V_y}{\partial x}$	$\mathbf{rot}\, \mathbf{V} = \frac{\partial V_r}{\partial z} - \frac{\partial V_z}{\partial r}$
$\Delta \mathbf{V} = (\Delta V_x, \Delta V_y)$	$\Delta \mathbf{V} = \left(\Delta V_r - \frac{1}{r^2} V_r, \Delta V_z\right)$

APPENDIX 2

Consider for example Maxwell equations (1). In the cylindrical case the finite volume formulation is

$$\frac{\partial}{\partial t}\left(\int_{V_i} B\right) - \sum_{k=1}^{N_i} \int_{\partial V_i^k} \mathbf{E} \cdot \boldsymbol{\tau}_i^k = 0$$

$$\frac{\partial}{\partial t}\left(\int_{\partial D_j^l} r\mathbf{E} \cdot \mathbf{v}_j^l\right) + c^2 \int_{\partial D_j^l} \mathbf{V}(rB) \cdot \boldsymbol{\tau}_j^l = -\frac{1}{\varepsilon_0} \int_{\partial D_j^l} r\mathbf{J} \cdot \mathbf{v}_j^l$$

$$\sum_{l=1}^{N_j} \int_{\partial D_j^l} r\mathbf{E} \cdot \mathbf{v}_j^l = \frac{1}{\varepsilon_0} \int_{D_j} r\rho,$$

or

$$\frac{\partial}{\partial t}\left(\int_{D_j} B\right) - \sum_{l=1}^{N_j} \int_{\partial D_j^l} \mathbf{E} \cdot \boldsymbol{\tau}_j^l = 0$$

$$\frac{\partial}{\partial t}\left(\int_{\partial V_i^k} r\mathbf{E} \cdot \mathbf{v}_i^k\right) + c^2 \int_{\partial V_i^k} \mathbf{V}(rB) \cdot \boldsymbol{\tau}_i^k = -\frac{1}{\varepsilon_0} \int_{\partial V_i^k} r\mathbf{J} \cdot \mathbf{v}_i^k$$

$$\sum_{k=1}^{N_i} \int_{\partial V_i^k} r\mathbf{E} \cdot \mathbf{v}_i^k = \frac{1}{\varepsilon_0} \int_{V_i} r\rho.$$

APPENDIX 3

The space discretization of Maxwell equations (2) by the finite volume methods described in Section 4.1 provides the following linear diagonal systems of differential equations:

$$L_j^l \frac{\partial}{\partial t}(\mathbf{B}\cdot\mathbf{v}_j^l) - E_{v(i,k)} + E_i = 0$$

$$A_i \frac{\partial E_i}{\partial t} - c^2 \sum_{k=1}^{N_i} L_i^k \mathbf{B}\cdot\tau_i^k = -\frac{1}{\varepsilon_0}\int_{\nu_i} J$$

$$\sum_{l=1}^{N_j} L_j^l \mathbf{B}\cdot\mathbf{v}_j^l = 0$$

and

$$L_i^k \frac{\partial}{\partial t}(\mathbf{B}\cdot\mathbf{v}_i^k) + E_{v(j,l)} - E_j = 0$$

$$A_j \frac{\partial E_j}{\partial t} - c^2 \sum_{l=1}^{N_j} L_j^l \mathbf{B}\cdot\tau_j^l = -\frac{1}{\varepsilon_0}\int_{D_j} J$$

$$\sum_{k=1}^{N_i} L_i^k \mathbf{B}\cdot\mathbf{v}_i^k = 0.$$

As for the continuous system (2), the last equation is a straightforward consequence of the first one and does not have to be considered.

ACKNOWLEDGMENT

We thank J. Segre for his fully vectorized particle code on unstructured triangular meshes. This code has been used for the simulation of both electron injector devices.

REFERENCES

1. R. W. Hockney and J. R. Eastwood, *Computer simulations using particles* (McGraw-Hill, New York, 1981).
2. C. K. Birdsall and A. B. Langdon, *Plasmas physics via computer simulation* (McGraw-Hill, New York, 1985).
3. B. Delaunay, *Bull. Acad. Sci. URSS Cl. Sci. Math. Nat.* **793** (1934).
4. F. Hermeline, Thesis, Université P. et M. Curie, 4 place Jussieu 75232, Paris Cédex 05, France, 1980 (unpublished).
5. F. Hermeline, *RAIRO Anal. numér.* **16**, no. 3, 211 (1982).
6. J. C. Cavendish, D. A. Field, and W. H. Frey, *Int. J. Methods Eng.* **21**, 329 (1985).
7. A. Perronnet, Tetracdrisation d'un objet multimatériaux ou de l'extérieur d'un objet, LAN 189, Université P. et M. Curie, 4 place Jussieu 75232, Paris Cédex 05, France, 1988 (unpublished).
8. T. J. Baker, *Second Int. Conf. on numerical grid generation in computational fluid dynamics, Miami Beach, Florida* (Pineridge Press, Swansea, 1988).
9. P. L. George and F. Hermeline, Maillage de Delaunay d'un polyèdre convexe en dimension *d*, Note CEA no. 2590, 1989 (unpublished).
10. G. Voronoi, *J. Reine Angew. Math.* **134**, 198 (1908).
11. H. S. M. Coxeter, L. Few, and C. A. Rogers, *Mathematika* **6**, 147 (1959).
12. C. L. Lawson, Software for c^1 surface interpolation, in *Mathematical software III* (Academic Press, New York/London, 1977), p. 161.
13. F. D. Preparata and M. I. Shamos, *Computational geometry, an introduction* (Springer-Verlag, New York/Berlin, 1985).
14. C. L. Lawson, *Comput. Aided Geom. Design* **3**, 231 (1986).
15. C. Cherfils and F. Hermeline, M^2AN **24**, no. 5, 613 (1990).
16. F. Hermeline, Deux schémas d'approximation des équations de Vlasov–Maxwell bidimensionnelles sur des maillages de Voronoï et Delaunay, Report CEA-N-2591, CEL-MA/MCN, 94195 Villeneuve, St Georges Cédex, France, 1989 (unpublished).
17. Z. J. Cendes, D. Shenton, and H. Shahnasser, *IEEE Trans. Magn.* **MAG-19**, no. 6, 2551 (1983).
18. B. J. McCartin and J. F. Dicello, *IEEE Trans. Magn.* **MAG-25**, no. 4, 3092 (1989).
19. M. S. Mock, *COMPEL* **2**, no. 3, 117 (1983).
20. T. Kojima, Y. Saito, and R. Dang, *IEEE Trans. Magn.* **25**, no. 4, 2953 (1989).
21. C. Börgers and C. Peskin, in *Proceedings, Int. Conf. on Free Lagrange Methods*, edited by M. J. Fritts et al., Lecture notes in Physics, Vol. 238 (Springer-Verlag, New York/Berlin, 1985).
22. R. A. Nicolaides, ICASE Report no. 89-76, 1989 (unpublished).
23. K. S. Yee, *IEEE Trans. Antennas Propag.* **14**, 302 (1966).
24. A. Taflove and K. R. Umashankar, *J. Elect. Wave Appl.* **1**, 243 (1987).
25. N. K. Madsen and R. W. Ziolkowski, *Wave Motion* **10**, 583 (1988).
26. N. K. Madsen and R. W. Ziolkowski, *Electromagnetics* **10**, 147 (1990).
27. J. C. Adam, A. Gourdin-Serveniere, J. C. Nedelec, and P. A. Raviart, *Comput. Methods* in *Appl. Mech. Eng.* **22**, 327 (1980).
28. J. C. Nedelec, *Numer. Math.* **35**, 315 (1980).
29. A. Bossavit, *Comput. Methods Appl. Mech. Eng.* **76**, 299 (1989).
30. P. Degond, F. Hermeline, P. A. Raviart, and J. Segre, A coupled particle-finite element method for the approximation of Vlasov–Maxwell equations (unpublished).
31. P. L. George, *Generation automatique de maillages* (Masson, Paris, 1991).
32. P. Lascaux and R. Theodor, *Analyse numérique matricielle appliquée à l'art de l'ingénieur* (Masson, Paris, 1987).
33. P. A. Raviart, "An analysis of particle methods", in *Numerical methods in fluid dynamics*, edited by F. Brezzi, Lectures notes in Math., Vol. 1127 (Springer-Verlag, Berlin, 1985).
34. P. A. Raviart, Méthodes particulaires, Ecole d'été d'analyse numérique EDF-INRIA, 1987 (unpublished).
35. B. Marder, *J. Comput. Phys.* **68**, 48 (1987).
36. J. Langmuir and K. T. Compton, Electrical discharges in gases. part II., Fundamental phenomena in electrical discharges, *Rev. Mod. Phys.* **3**, 191 (1931).
37. P. Degond and P. A. Raviart, An asymptotic analysis of the one-dimensional Vlasov–Poisson system: The Child–Langmuir law, Centre de mathématiques appliquées, Ecole polytechnique, 91128 Palaiseau Cédex, France (1989).
38. E. Heintze, Internal report DO-1238, CEL BP 27, 94190 Villeneuve, St. Georges, France, 1989 (unpublished).
39. J. R. Pierce, *Theory and design of electrons beams*, 2nd ed., (Van Nostrand, New York, 1954).
40. T. Westermann, *Nucl. Instrum. Methods Phys. Res. Sect. A* **263**, 271 (1988).
41. P. Ravier and J. P. Penicaud, *Comput. Methods Appl. Mech. Eng.* **75**, 531 (1989).
42. R. Dei-Cas, *Nucl. Instrum. Methods Phys. Res. Sect. A* 304, 215 (1991).